Topology-aware permeability modeling in structured porous media for passive flow control

By S. Lee AND S. Vijay

Classical permeability models are limited in capturing pore-scale topological effects on flow behavior. To enable topology-aware design of structured porous media for applications such as passive flow control, this report introduces a data-driven framework integrating generative design, numerical simulation, and machine learning. The framework combines a Design-by-Morphing (DbM) technique for generating diverse 3D topologies, direct numerical simulations for permeability evaluation, and Bayesian optimization (BO) with Gaussian process (GP) surrogate modeling for sample-efficient exploration of the design space. A proof-of-concept study is presented to demonstrate the capability of the framework. The framework facilitates topology-aware permeability modeling and inverse design of porous media, offering insights for near-wall turbulence control research.

1. Introduction

Turbulent flow control is a critical objective in many engineering fields, offering potential for drag reduction, enhanced heat transfer, and reduction in aerodynamic noise, among many applications. Recent efforts have shown that anisotropic patterned porous surfaces have shown significant promise in achieving drag reduction and enhanced heat transfer. Using the virtual origin framework of riblets proposed by Luchini (1996), previous studies have shown that substrates for which the permeability $\mathbf{K} = (\kappa_{ij})$ is higher in the streamwise direction (κ_{xx}) as compared to the spanwise (κ_{zz}) and wall-normal (κ_{yy}) direction, also known as streamwise preferential substrates, are promising candidates for passive drag reduction. In this framework, the virtual origin perceived by a mean flow is defined as the location where the quasi-streamwise near-wall vortices perceive a non-slipping wall and are attributed to the offset between streamwise slip length ℓ_U^+ and a transverse slip length ℓ_T^+. A superscript + denotes normalization with respect to the friction velocity u_τ and kinematic viscosity ν. A generalization of this framework for anisotropic porous surfaces has revealed that streamwise and spanwise permeabilities can be related to the slip lengths as $\ell_x^+ \approx \sqrt{\kappa_{xx}}^+$ and $\ell_z^+ \approx \sqrt{\kappa_{zz}}^+$ for deep substrates, i.e., for $H^+ \gg \ell_U^+$ where H is the thickness of the porous substrate (García-Mayoral *et al.* 2019). This implies $\Delta U^+ \propto \sqrt{\kappa_{xx}}^+ - \sqrt{\kappa_{zz}}^+$, or that drag reduction can be achieved with anisotropic materials with a large streamwise-to-spanwise anisotropy ratio, $\phi_{xz} = \kappa_{xx}/\kappa_{zz} > 1$. Linear stability analyses suggest that performance deterioration is observed when the normalized wall-normal permeability exceeds a certain threshold, $\sqrt{\kappa_{yy}}^+ \gtrsim 0.4$. Thus, for drag reduction to be achieved, the material must exhibit streamwise-preferential slip as well as low wall-normal permeability. More recent experimental efforts have shown that although slip lengths depend on permeability, they also might depend on the specific interfacial geometry (Vijay & Luhar 2024).

Classical models, such as Darcy's linear law and its nonlinear extension, the Forchheimer equation (e.g., Nield 2009), provide a constitutive relationship between the applied pressure gradient and the resulting superficial flow velocity (i.e., Darcy velocity). While

foundational, these models assume that permeability is a bulk, homogenized property, which may obscure the specific geometric features at the pore scale. According to Gómez-de-Segura & García-Mayoral (2019), through their extensive experimental campaign on anisotropic cubic lattices, drag reduction did not occur for geometries that were expected to show drag reduction. This can be attributed to a decreased effective slip length for the streamwise mean flow. With the advent of modern additive manufacturing, architected microstructures have become feasible, and this geometric dependence could represent a critical missing link for precise structure design. A central challenge, therefore, is not only to establish a robust constitutive relationship between the microtopology of a porous medium and its bulk properties, such as permeability, but also to resolve and tune pore-scale geometries to better design anisotropic structures and understand their influence on properties such as slip length for drag reduction.

To address the limitations of classical, geometrically blind models, we introduce a topology-aware, data-driven framework for the systematic design and analysis of structured porous media. First, Design-by-Morphing (DbM) (Sheikh *et al.* 2023), a powerful, training-free design generation technique, creates an extensive and continuous design space from known baseline topologies via morphing. We incorporate Signed Distance Functions (SDFs) (e.g., Benjamin & Iaccarino 2025) into the DbM morphing process to produce novel and complex structured porous geometries in 3D. Direct numerical simulations of creeping flows in the pores are then conducted to evaluate the performance of any given geometry, including its permeability. Lastly, Bayesian optimization (BO) is employed to efficiently explore the vast and computationally expensive design–performance map. This integrated approach, previously utilized for riblet-surface turbulent drag reduction (Lee *et al.* 2024), is applied here to enable the systematic discovery of intricate structure–property relations, constituting a data-driven framework for understanding the geometric dependencies of permeability.

The remainder of this report is structured as follows. Section 2 provides background on structured porous media and morphing-based topology design. Section 3 details the data-driven design framework, including the numerical methods and optimization strategy. Section 4 presents results from a proof-of-concept design exploration aimed at maximizing both permeability and specific surface area. Finally, Section 5 discusses the conclusions, implications for turbulence research, and future work.

2. Background

2.1. *Permeability and its relationship to microstructure*

Permeability, $\mathbf{K}$, quantifies the resistance to flow offered by the media. In the Stokes flow limit, this relationship is captured by Darcy's law, where the superficial (volume-averaged) velocity $\langle \mathbf{u} \rangle$ and the pressure gradient ∇p satisfy

$$\nabla p = -\mu \, \mathbf{K}^{-1} \langle \mathbf{u} \rangle, \tag{2.1}$$

where μ is the fluid's dynamic viscosity. In general, $\mathbf{K}$ is a second-order tensor, reflecting directional dependence (i.e., anisotropy) (Liakopoulos 1965). For an isotropic medium, where permeability is the same in all directions, the tensor simplifies to a scalar K, and the velocity vector becomes parallel to the pressure gradient. As flow velocities increase, inertial effects become significant, and the relationship is often described with non-linear terms (Nield 2009).

Conventional approaches to understanding permeability in relation to microstructure

have been agnostic in geometry. Previous endeavors to evaluate permeability have been driven by interests in soil engineering, hydraulics, and petroleum engineering, particularly focusing on granular samples with low porosity (e.g., the Kozeny–Carman equation). Furthermore, only a limited number of studies have provided data beyond the primary component of the permeability tensor. However, these macroscopic laws are empirical or phenomenological, and their coefficients are effective parameters that encapsulate the integrated effects of microscale fluid dynamics.

In the context of multifunctional flow control, Vijay (2023) reports experimentally measured permeability values for anisotropic cubic unit cells using a benchtop permeameter. More recently, Aghaei-Jouybari *et al.* (2024) demonstrated that the classical Darcy–Forchheimer law holds for isotropic media, but that anisotropy introduces a misalignment between the pressure gradient and the resulting flow direction at higher Reynolds numbers—a phenomenon they term inertial flow deflection. Their findings suggest that the modeling of the Forchheimer term must account for this deflection to accurately capture nonlinear inertial effects. Furthermore, topologically distinct geometries can exhibit the same nominal permeability, and growing evidence indicates that pore geometry can also influence effective slip lengths.

2.2. *Morphing-based topology design*

The findings outlined above raise an important inverse-design question; given a target permeability tensor or flow constraint, can a design search process identify a physically realizable geometry that satisfies the goal? Here, we introduce morphing-based topology design as a systematic tool to explore and generate such geometries within the feasible design space.

DbM is a training-free generative design approach that constructs a continuous and expansive design space from a small set of known baseline shapes of size $N \sim \mathcal{O}(10^0 - 10^1)$. While the principles and philosophy of the approach are explained in the literature (Sheikh *et al.* 2023; Lee *et al.* 2024), the fundamental concept involves generating a novel design as a weighted morphing of the baseline shapes, permitting negative weights (i.e., extrapolation).

To apply this to topologically distinct 3D objects, we employ SDFs as the underlying geometric representation. For a given shape Ω with boundary $\partial\Omega$ in a metric space, its SDF is an implicit function, $S(\mathbf{x}) : \mathbb{R}^3 \to \mathbb{R}$, defined as

$$S(\mathbf{x}) = \begin{cases} -d(\mathbf{x}, \partial\Omega) & \text{if } \mathbf{x} \in \Omega, \\ d(\mathbf{x}, \partial\Omega) & \text{if } \mathbf{x} \notin \Omega \end{cases} \tag{2.2}$$

where $d(\mathbf{x}, \partial\Omega) = \inf_{\mathbf{y}\in\partial\Omega} \|\mathbf{x} - \mathbf{y}\|_2$ is the minimum Euclidean distance from a point $\mathbf{x}$ to the shape boundary. The surface itself is then described as the zero-level set, $S(\mathbf{x}) = 0$.

With the topology mapped to a function via SDF, where mathematical operations are well-defined, the morphing can be formally expressed as a weighted sum. The SDF of a new, morphed shape S_{morphed} is generated from N baseline SDFs S_i $(i = 1, \cdots, N)$, using a set of corresponding weights w_i, i.e.,

$$S_{\text{morphed}}(\mathbf{x}; \mathbf{w}) = \sum_{i=1}^{N} w_i S_i(\mathbf{x}), \tag{2.3}$$

where $\mathbf{w} = (w_1 \ \cdots \ w_N)^T$. The weights take either positive or negative values ($w_i \in [-1, 1]$), enabling both interpolative morphing (when all weights are non-negative) and

extrapolative morphing (when some weights are negative), thus significantly expanding the reachable design space beyond the convex hull of the baseline shapes.

This formulation creates an N-dimensional design space spanned by the weight vector $\mathbf{w}$. Since the zero-level set of $S_{\text{morphed}}(\mathbf{x}; \mathbf{w})$ and that of $S_{\text{morphed}}(\mathbf{x}; c\mathbf{w})$ for any non-zero constant c are fundamentally the same, only the direction of $\mathbf{w}$ matters. This allows the design space to be constrained to the surface of an $(N-1)$-dimensional unit hypersphere, reducing the design-space dimensionality by one. This hypersphere can be parameterized using $(N-1)$ angular coordinates $(\varphi_1, \cdots, \varphi_{N-1})$. The weights w_i are related to the angular coordinates by the transformation of

$$\begin{aligned} w_1 &= \cos(\varphi_1), \\ w_2 &= \sin(\varphi_1)\cos(\varphi_2), \\ &\vdots \\ w_{N-1} &= \sin(\varphi_1)\cdots\sin(\varphi_{N-2})\cos(\varphi_{N-1}), \\ w_N &= \sin(\varphi_1)\cdots\sin(\varphi_{N-2})\sin(\varphi_{N-1}), \end{aligned} \tag{2.4}$$

where $\varphi_1, \cdots, \varphi_{N-2} \in [0, \pi]$ and $\varphi_{N-1} \in [0, 2\pi]$. This hypersphere parameterization inherently handles the normalization of the weight vector w.

The use of SDFs for DbM offers several advantages over traditional approaches (e.g., one-to-one surface point mapping). First, SDF interpolation naturally handles changes in topology, such as the merging or splitting of struts and the creation or closure of pores, which is a critical capability for discovering truly novel and potentially superior topologies that are inaccessible through conventional parameterization. Second, a SDF provides a continuous, volumetric representation of the geometry that is mathematically robust and guarantees the generation of a watertight surface.

While the surface is typically defined by the default zero-level set ($S_{\text{morphed}}(\mathbf{x}) = 0$), the level-set value s can be considered an additional design variable, providing another degree of freedom. In the present context of structured porous media, slightly adjusting s from zero effectively offsets the surface, which thickens the structure's struts or wanes them, yielding direct and intuitive control over the overall porosity of the lattice.

3. Methodology

3.1. *Data-driven design search framework*

The core of our methodology is a closed-loop, data-driven framework for the efficient exploration and optimization of the vast design space for structured porous media generated by DbM. The overall workflow, illustrated in Figure 1, begins with a set of baseline shapes and iteratively builds a surrogate model of the performance space to adaptively guide the search for high-impact designs. The DbM module generates new candidate designs through weighted morphing of the baselines. Each generated design then undergoes a feasibility check to remove any physically unrealizable geometries, such as those containing floating solid volumes, which are infeasible for manufacturing.

It is noted that engineered porous media with a structured, lattice-based architecture are defined by the periodic arrangement of a repeating unit cell. This regularity, which has been made feasible by advances in additive manufacturing, allows for precise control over thermophysical properties. While the repeating unit cell structure makes the media homogeneous on a macroscopic scale, the permeability can be either isotropic (directionally independent) or anisotropic (directionally dependent); this proof-of-concept study

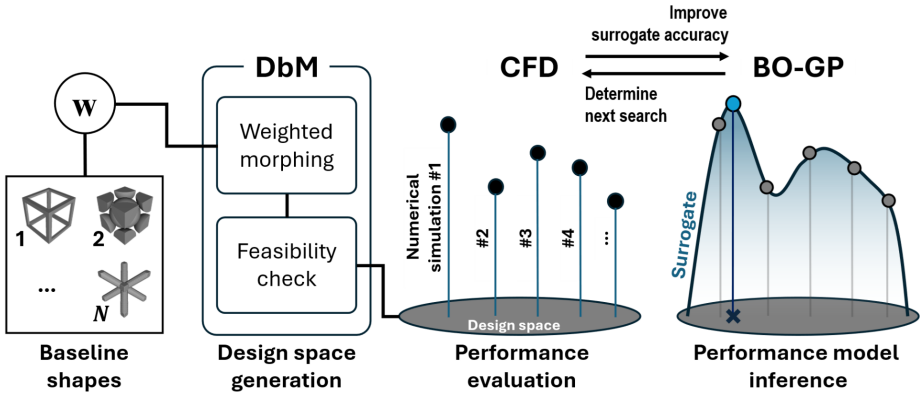

FIGURE 1. Flowchart of the data-driven design search framework.

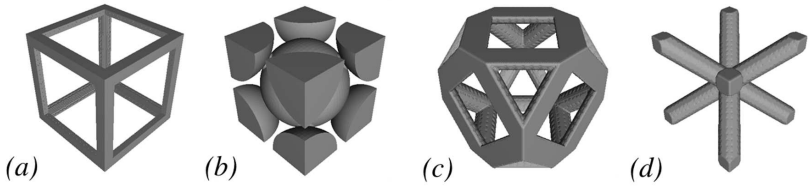

FIGURE 2. Examples of unit lattice geometries for structured porous media. From left to right: (a) cubic, (b) body-centered cubic (BCC) sphere, (c) Kelvin cell and (d) cross.

focuses on isotropic cases by using isotropic baselines. Some key macroscopic properties are defined as follows: Porosity ϵ is the dimensionless ratio of the void volume to the total volume of the medium. The specific surface area S_a is the total fluid–solid interface area per unit volume, a critical parameter for applications involving heat transfer or chemical reactions.

For the proof-of-concept study presented in this report (Section 4), we make use of the four isotropic lattice geometries shown in Figure 2—cubic, BCC sphere, Kelvin cell, and cross—as baselines ($N = 4$). These geometries were retrieved from the open-source Porous Microstructure Generator (PMG) (Niblett *et al.* 2024). It should be noted that for more comprehensive research, a larger and more diverse set of known lattice structures could be chosen, and non-equal aspect ratios could be introduced to account for anisotropy. With four baselines, the design space is spanned by three angular coordinates (φ_1, φ_2, φ_3) and the level-set value s, which varies within a narrow range of $[-0.2, 0.2]$ for slight adjustments to strut thickness. The performance of each design is evaluated based on two objectives: permeability K and specific surface area S_a.

Feasible designs form the resulting design space (see Figure 3 for examples) and are passed to the performance evaluation stage, where computational fluid dynamics (CFD) simulations are used to compute their properties (detailed in the following subsection). The resulting data points—design parameters and their corresponding performance—are used to build and iteratively improve a surrogate performance model via BO with a GP surrogate. The BO-GP stage determines the next most informative design candidate to evaluate, balancing the exploration of new, uncertain regions of the design space with the exploitation of known high-performance zones. This new candidate is fed back into

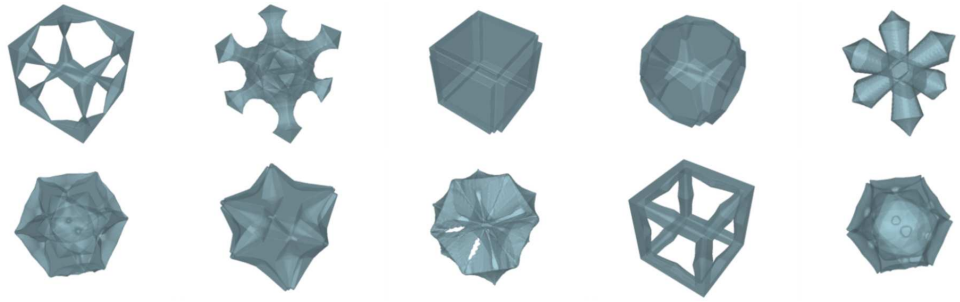

FIGURE 3. Examples of new unit lattice designs obtained via random morphing.

the CFD evaluation stage, closing the loop and progressively enhancing the surrogate model's accuracy.

The iterative sampling of the design space is conducted using BoTorch with the qLogNEHVI acquisition function (Ament *et al.* 2023), after preliminary tests with the ZDT1–3 functions (Zitzler *et al.* 2000). The goal is to enhance the accuracy of the surrogate performance model as quickly as possible, particularly in what the user defines as "better-performing designs." The definition of "better-performing" depends on the specific design optimization goals. If one solely desires a wider survey of the design space, they can tune the BO-GP module to favor more aggressive exploration over exploitation.

3.2. *Permeability calculation*

The hydraulic permeability K and specific surface area S_a of each generated lattice structure are determined through geometric analysis and direct numerical simulation. First, the structure's SDF is converted to a surface geometry format (STL), from which the specific surface area S_a is calculated by summing the area of all triangular faces that constitute the fluid–solid interface.

To calculate permeability, the flow of an incompressible, viscous fluid (density ρ and dynamic viscosity μ) through the unit cell is simulated using the open-source CFD package OpenFOAM. The simulation solves the steady-state, incompressible Navier–Stokes equations in the low-speed regime, where the Reynolds number $Re = \rho U_d L_c/\mu < 1$ (U_d is the Darcy velocity magnitude and L_c is the cell size). The computational domain, representing the fluid volume within the unit cell, is meshed using the snappyHexMesh utility to create a body-fitted grid. To simulate an infinite porous medium, periodic boundary conditions are applied to all three pairs of opposing faces. A constant volumetric body force is applied in the x direction to represent a constant pressure gradient p_x, which drives the flow, and a no-slip condition is enforced on the lattice surface.

Once the simulation converges to a steady-state solution, the Darcy velocity U_d is computed by volume-averaging the velocity field over the entire unit cell. The permeability K is then calculated from the linear proportionality between U_d and p_x, as defined by Darcy's law as in Eq. (2.1) (n.b. the present proof-of-concept study focuses on low-speed, isotropic cases). To ensure the flow remains in the linear Darcy regime, the system is characterized by two dimensionless parameters: the Reynolds number, Re, and a pressure gradient parameter, $\mathit{\Pi} = -(p_x L_c^3)/(\mu^2/\rho)$. Rearranging Darcy's law in non-dimensional form yields

$$\frac{K}{L_c^2}\mathit{\Pi} = Re. \tag{3.1}$$

Porous lattice type	**Our permeability (Normalized by L_c^2)**	**Vijay & Luhar (2024) (Normalized by L_c^2)**
HHH	0.043	0.088 ± 0.022
MMM	0.030	0.026 ± 0.004
LLL	0.024	0.035 ± 0.005

TABLE 1. Comparison of the numerical simulations against literature data.

For all simulations, we constantly set $\Pi = 1$ by choosing $p_x = -(\mu^2/\rho)/L_c^3$. Since the dimensionless permeability K/L_c^2 (often called the Darcy number) for typical porous media is much less than 1, this setup guarantees that the resulting Reynolds number is also much less than 1, validating the low-speed assumption.

Beyond the proof-of-concept study in this report, it is worthwhile to note that the framework can be readily extended to determine the full anisotropic permeability tensor at higher Reynolds numbers, where K/L_c^2 would become a nonlinear function of Re and Π. Future work will explore such nonlinear influences in permeability modeling.

In Table 1, we compare experimentally measured permeability values from Vijay & Luhar (2024) and OpenFOAM simulations for isotropic cubic unit cells. Here, each cube is referenced by a three-letter combination, each denoting the cube size in x, y, and z direction, respectively, with H = 3 mm, M = 2 mm, and L = 1.5 mm for L_c. For all cases, the strut thickness is kept constant at 0.4 mm. Experimental values are obtained using an in-house permeameter (refer to Vijay & Luhar (2024) for more details on the experimental setup and procedure).

For all cases, it can be observed that the computed permeability values are in the same order of magnitude as the corresponding literature data. However, the values between experiments and simulations differ in the range of 15–50%. As further discussed in detail in Vijay (2023), measured values of strut thicknesses in the experiment indicate up to 20% variation from the nominal design in some cases due to manufacturing tolerances. This variation in sizes and clogging of pores can result in different values of permeability than those computed from numerical models. These observations highlight the limitations of physically realizable geometries in determining permeability, emphasizing that additive manufacturing constraints must be considered when predicting and designing porous materials.

Rather than treating these deviations as purely experimental uncertainty, the DbM framework provides a means to systematically explore such variations within the parameter space. By accounting for geometric sensitivity directly in the design loop, DbM enables fine-tuning of microstructural features to achieve target permeability values, making the design process both more predictive and more adaptable to real-world fabrication constraints.

4. Proof-of-concept study

To demonstrate the capability of the proposed framework, a proof-of-concept study was conducted to explore the design space of isotropic porous lattices. The design search process was initialized with 40 randomly sampled designs and then run for an additional 460 iterations guided by the BO-GP algorithm, for a total of 500 CFD evaluations. The

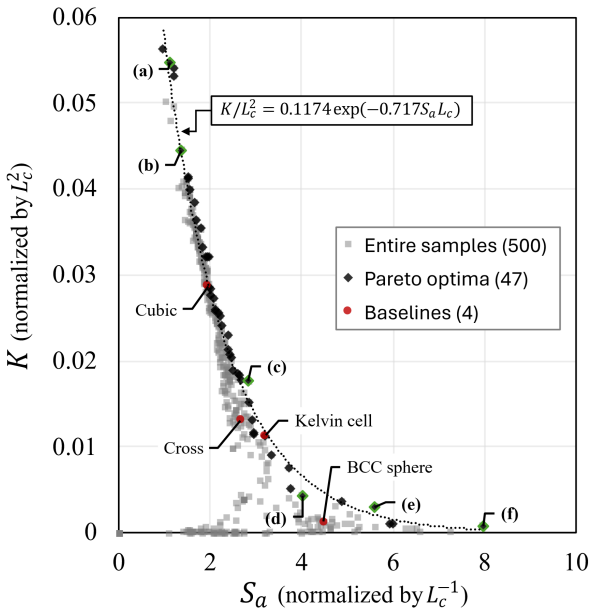

FIGURE 4. Data-driven design search results showing all 500 samples. The 47 Pareto-optimal design points are marked as black diamonds. The four baseline designs are shown as red circles. The designs corresponding to the points with green strokes are shown in Figure 5.

objective was to identify high-impact designs by simultaneously optimizing for permeability (K) and specific surface area (S_a).

Throughout this process, the framework builds a GP surrogate performance model that becomes particularly accurate in regions of high performance. Mathematically, the surrogate model establishes the relation $\mathbf{F}$, which is

$$\underbrace{\begin{pmatrix} K/L_c^2 \\ S_a L_c \end{pmatrix}}_{\substack{\text{perform.} \\ \text{outputs}}} = \mathbf{F}(\underbrace{\varphi_1, \varphi_2, \varphi_3, s}_{\substack{\text{topology} \\ \text{inputs}}}). \tag{4.1}$$

This relation explicitly connects the topological variation of unit lattice designs—defined by the DbM variables (φ_i's and s)—to the systematic properties—dynamic (K/L_c^2) and geometric ($S_a L_c$)—that define the design's performance, enabling a comprehensive, topology-aware permeability model.

A useful way to interpret the model $\mathbf{F}$ is to project it onto the performance metric space of $(K/L_c^2, S_a L_c)$. Figure 4 shows all 500 design evaluations in this space, revealing 47 non-dominated designs that form the Pareto front, which defines the optimal trade-off between the objectives. The BO process adaptively samples near this frontier, leading to a progressively more precise definition of the performance limits. This frontier provides insight into the limits of achievable performance, and a mathematical fit can serve as a useful proxy model, analogous to classical models that relate only bulk properties. For instance, as shown in Figure 4, the performance limit of K/L_c^2 with respect to $S_a L_c$ is found to be

$$\frac{K}{L_c^2} = 0.1174 \exp\left(-0.717(S_a L_c)\right) \tag{4.2}$$

which relates the bulk geometric property to the dynamic performance of the system.

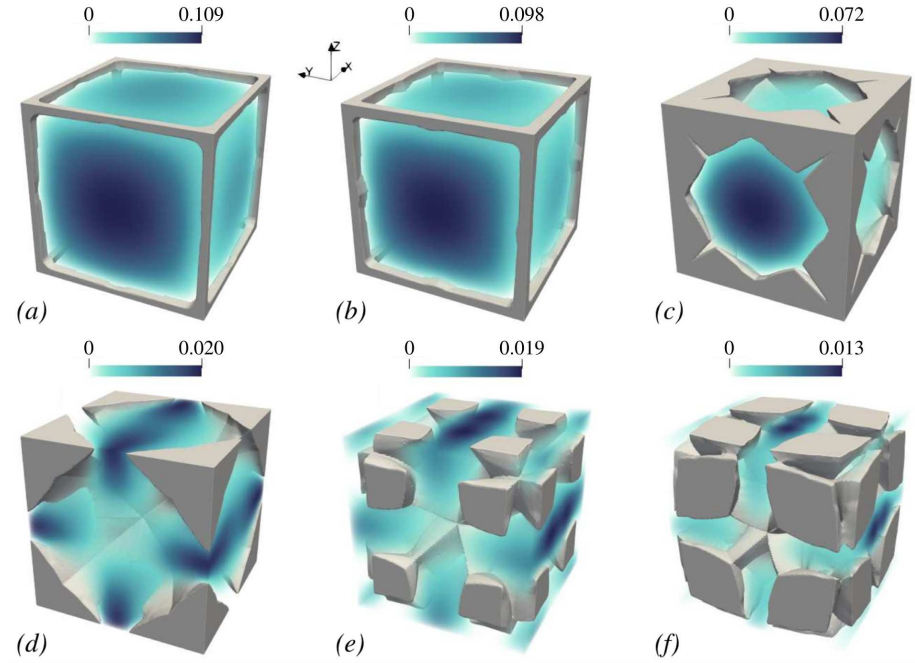

FIGURE 5. Representative unit lattice designs from the Pareto front (marked with green strokes in Figure 4), each shown with the velocity magnitude field contour (normalized by $\mu/(\rho L_c)$). The performance values ($K/L_c^2,\ S_a L_c$) are (a) (0.0547, 1.125), (b) (0.0446, 1.374), (c) (0.176, 2.847), (d) (0.0043, 4.106), (e) (0.0030, 5.595), and (f) (0.0008, 7.961).

The strength of the topology-aware model **F** lies in its ability to link any point on the performance front back to the specific unit lattice design that produces it. Figure 5 displays six representative unit lattice designs from the Pareto front. Examining the topological variance across these optimal designs provides deeper insights than analyses based solely on homogenized, bulk properties. The designs are shown from top-left to bottom-right in descending order of permeability.

Several key observations can be made:

- Designs with higher permeability (top row) are dominated by features from the cubic baseline, while those with larger surface area (bottom row) show a stronger influence from topologically more complex baselines like the BCC sphere and Kelvin cell.
- The Kelvin cell baseline design lies on the Pareto front. Although it is outperformed by the cubic baseline in permeability and by the BCC sphere in surface area, it represents a balanced solution achieving moderate performance in both objectives.
- The cross baseline is dominated by the other three baselines in the performance space. Consequently, its influence on the final Pareto-optimal designs is minimal, with its corresponding weight factor typically being the smallest.

Last but not least, a key finding is the considerable sensitivity of permeability to subtle geometric variations, exemplified by comparing the two nearly cubic designs in Figure 5(a, b). Although their overall geometries appear nearly identical, the resulting permeability values differ by nearly 20% (0.0547 vs. 0.0446). This observation sheds light on the challenges in designing porous materials to precise specifications (e.g., Rosti *et al.* 2015) and provides a physical basis for discrepancies observed between CFD calculations and

experimental measurements. During additive manufacturing, inevitable, minor defects, such as slight variations in strut thickness or small, unintended material deposits, are analogous to the subtle topological variations between the designs in Figure 5(a, b). This suggests that experimental uncertainty in manufactured lattice structures can be larger than anticipated due to these hidden sensitivities affecting the resulting permeability.

5. Conclusion and future work

This report introduced an integrated framework for the topology-aware design and modeling of structured porous media. By coupling a generative Design-by-Morphing method with CFD simulation and Gaussian process surrogate modeling powered by Bayesian optimization, we created a powerful tool for exploring complex structure–property relationships. The proof-of-concept study for low-speed, isotropic unit lattices successfully explored designs that balance permeability and specific surface area, forming a reliable model connecting lattice topology to its performance. A key finding from this study is the high sensitivity of permeability to subtle geometric variations, a finding that is expected to explain the high permeability uncertainties observed in experiments by relating them to manufacturing defects.

Building on this successful proof of concept, the framework can be extended to establish a more generalized constitutional model. The surrogate performance model $\mathbf{F}$ can be expanded to incorporate a wider range of physical parameters, moving beyond the current study. The generalized form of $\mathbf{F}$ we envision for future work is

$$\begin{pmatrix}\text{dynamic properties}\\ \text{geometric properties}\end{pmatrix} = \mathbf{F}(\text{topology variables, flow variables}). \tag{5.1}$$

This generalized model allows for a more comprehensive exploration of the design space. For dynamic properties, we can move beyond the linear Darcy regime by treating permeability not as an intrinsic constant but as a varying quantity. The model's dynamic property output could become the pressure drop or drag (represented by Π), while the flow variable inputs would include a more extensive range of Reynolds numbers (Re) to capture non-linear flow effects. For geometric properties, the model can be enriched to include additional bulk characteristics beyond specific surface area, such as porosity ϵ. This would provide deeper insights into the macroscopic relationships between bulk geometry and dynamic performance.

Ongoing work involves extending this framework to explicitly account for anisotropy. In addition to the DbM variables that control the fundamental topology, parameters such as width-to-height and width-to-span aspect ratios can be introduced as inputs to the model. This would allow for the design of directionally dependent structures, where the permeability becomes a tensor, $\mathbf{K}$, with multiple components. This will eventually allow us to predict *a priori* a porous microstructure that may satisfy $\kappa_{xx}^{+} \gg \kappa_{zz}^{+}$ with $\kappa_{yy}^{+} < 0.4$ to help predict a physically realizable design for a drag-reducing substrate.

The capabilities of this generalized framework are expected to offer a path toward addressing challenges in passive turbulent flow control. The effectiveness of porous surfaces in attenuating turbulence is governed by their ability to impose specific slip and penetration conditions, which are a function of both topology and flow conditions. By establishing a robust, data-driven mapping from topology and flow variables to dynamic response, our framework provides the foundational tool for the inverse design problem: engineering a specific microgeometry to achieve a target performance. This opens the

door to designing functionally graded porous substrates with spatially varying topologies, tailored to manipulate specific turbulent structures with unprecedented precision. Future work to incorporate heat conduction is planned to also couple conjugate heat transfer performance as an aspect of flow control.

Acknowledgements

The support of ONR to CTR under grant N000142312833 is gratefully acknowledged.

REFERENCES

Aghaei-Jouybari, M., Seo, J.-H., Pinto, S., Cattafesta, L., Meneveau, C. & Mittal, R. 2024 Extended Darcy–Forchheimer law including inertial flow deflection effects. *J. Fluid Mech.* **980**, A13.

Ament, S., Daulton, S., Eriksson, D., Balandat, M. & Bakshy, E. 2023 Unexpected improvements to expected improvement for Bayesian optimization. *Adv. Neural Inf. Process. Syst.* **36**, 20577–20612.

Benjamin, M. & Iaccarino, G. 2025 A systematic dataset generation technique applied to data-driven automotive aerodynamics. *APL Mach. Learn.* **3**, 016110.

García-Mayoral, R., Gómez-de-Segura, G. & Fairhall, C. T. 2019 The control of near-wall turbulence through surface texturing. *Fluid Dyn. Res.* **51**, 011410.

Gómez-de-Segura, G. & García-Mayoral, R. 2019 Turbulent drag reduction by anisotropic permeable substrates – analysis and direct numerical simulations. *J. Fluid Mech.* **875**, 124–172.

Lee, S., Sheikh, H. M., Lim, D. D., Gu, G. X. & Marcus, P. S. 2024 Bayesian-optimized riblet surface design for turbulent drag reduction via Design-by-Morphing with large eddy simulation. *J. Mech. Des.* **146**, 081701.

Liakopoulos, A. C. 1965 Darcy's coefficient of permeability as a symmetric tensor of second rank. *Trans. ASAE* **8**, 0216–0218.

Luchini, P. 1996 Reducing the turbulent skin friction. In Désidéri J. A. et al. (Eds.), *Computational Methods in Applied Sciences' 96* (pp. 465–470), Wiley.

Niblett, D., Mamlouk, M., Godinez-Brizuela, O. E. & An, S. 2024 *Porous Microstructure Generator* (Version 2.0) [Software]. Newcastle University.

Nield, D. A. 2009 The modeling of form drag in a porous medium saturated by a power-law fluid. *J. Heat Transf.* **131**, 104501.

Rosti, M. E., Cortelezzi, L. & Quadrio, M. 2015 Direct numerical simulation of turbulent channel flow over porous walls. *J. Fluid Mech.* **784**, 396–442.

Sheikh, H. M., Lee, S., Wang, J. & Marcus, P. S. 2023 Airfoil optimization using Design-by-Morphing. *J. Comput. Des. Eng.* **10**, 1443–1459.

Vijay, S. 2023 Flow and thermal transport at porous interfaces. PhD thesis, University of Southern California.

Vijay, S. & Luhar, M. 2024 Pressure drop measurements over anisotropic porous substrates in channel flow. *Exp. Fluids* **65**, 135.

Zitzler, E., Deb, K. & Thiele, L. 2000 Comparison of multiobjective evolutionary algorithms: empirical results. *Evol. Comp.* **8**, 173–195.